Mining Science, vol. 31, 2024, 39–59

www.miningscience.pwr.edu.pl

Mining Science

(Previously Prace Naukowe Instytutu Gornictwa Politechniki Wroclawskiej, ISSN 0370-0798)

ISSN 2300-9586 (print)
ISSN 2353-5423 (online)

Received December 27, 2023; Reviewed; Accepted August 23, 2024

STUDY ON THE FREEZE-THAW DAMAGE CHARACTERISTICS OF SKARN BASED ON CT THREE-DIMENSIONAL RECONSTRUCTION

Zhixin SHAO[1, 2], Yanqi SONG[1, 2]*, Fuxin SHEN[2], Hongfa MA[2], Junjie ZHENG[2], Juntao YANG[2]

[1] State Key Laboratory of Coal Resources and Safe Mining, China University of Mining and Technology (Beijing), Beijing,100083, China

[2] School of Mechanics and Civil Engineering, China University of Mining and Technology (Beijing), Beijing, 100083, China

Abstract: To study the mesoscopic damage evolution characteristics of skarn under freeze-thaw cycles, based on CT technology, the skarn samples under freeze-thaw action were scanned by CT, and the image data of skarn were segmented by Avizo software. The digital model of the three-dimensional structure of skarn was established, and the evolution law of the internal structure of skarn during the freeze-thaw cycle was quantitatively analyzed. The box dimension algorithm calculates the fractal dimension of the pore structure under freeze-thaw conditions. The relationship between fractal dimension, pore volume fraction, and freeze-thaw cycles was studied. According to the statistical results of the pore size distribution of skarn, the change characteristics of pore structure in the rock under the influence of freeze-thaw were studied. Based on the theory of rock damage mechanics, the damage variable of skarn was defined using the concept of the effective bearing zone, and the freeze-thaw damage evolution of skarn was studied. The results show that the three-dimensional reconstructed model can directly show each medium's meso-pore structure and spatial distribution. There is a positive correlation between pore volume fraction and fractal dimension under freeze-thaw conditions. The fractal dimension satisfies the exponential growth law. The skarn damage variable increases with the increase of freeze-thaw cycles, which is consistent with the development trend of pore structure. The exponential function can better reflect the damage evolution of skarn under freezing and thawing.

Keywords*: *skarn rock; freeze-thaw cycle; CT scan experiment; mesoscopic damage; damage variable

* Corresponding author: songyq1269@163.com (Y. Song)

doi: 10.37190/msc243103

1. INTRODUCTION

In recent years, extreme weather conditions have occurred frequently around the world. Low temperatures and snowy climates often affect mineral exploitation in cold regions. Xinjiang is one of the western provinces in China. Among the existing minerals found in the country, Xinjiang occupies three-quarters. Due to the characteristics of low temperature and air pressure in this area, the mining conditions are poor, and the disaster mechanism is complex. Freeze-thaw damage poses a significant threat to rock engineering. The surrounding rock of the mine in this area mainly includes skarn and tuff, with a small amount of sandstone. Affected by complex freeze-thaw environmental conditions, the physical and mechanical properties of rock will degrade, which will cause significant disasters. Therefore, it is of great significance to study the deterioration mechanism of freeze-thaw damage of rock mass for engineering construction, construction, and safe operation in cold regions.

In nature, rock is a material containing natural pores and fissures. During the freezing process, due to the volume expansion of the water-ice phase transition and the migration of unfrozen water, enormous pressure will be generated in the pores, causing pore cracking and primary fissure expansion. In the thawing stage, pore water seeps into the new pores, creating conditions for subsequent freezing cracking. (Tan et al. 2011a; 2011b; Wang et al. 2019) Many scholars have studied the damage and failure characteristics of rock mass under freeze-thaw conditions theoretically and experimentally (Nicholson et al. 2000; Bayram 2012; Cardenes et al. 2014; Javad Eslami et al. 2018) Zhang et al. (2018) and Qiao et al. (2021) studied the attenuation degree of rock physical and mechanical parameters by using intact rock and fractured rock for freeze-thaw cycles, respectively. Yan et al. (2015) analyzed the relationship between crack length and frost pressure in the rock under freeze-thaw conditions and established an elastoplastic damage model. Huang et al. (2018) proposed a theoretical model to calculate the unfrozen water content by strain, considering the phase transition of water ice during freezing and thawing. On this basis, Lv et al. (2022) proposed a thermodynamic coupling model of the freeze-thaw deformation of porous rock. Considering the characteristics of saturation and pore size distribution, Huang et al. (2021a; 2021b) established a frost heave model that can predict rock deformation and verified the rationality of the model by sandstone and cement slurry experiments. Gao et al. (2020) and Wang et al. (2021) focused on rock damage evolution and energy dissipation mechanism during the freeze-thaw process.

In recent years, various non-destructive testing methods to study the damage evolution mechanism of rock from the mesostructure have gradually become hot spots. Fener and Ince (2015) studied the texture changes of andesite during the freeze-thaw process with a polarizing microscope. Park et al. (2015) combined scanning electron microscopy (SEM) and computed tomography (CT) to study the changes in the internal micro-

structure of diorite, basalt, and tuff with freeze-thaw cycles. Zhou et al. (2015) studied the effects of freeze-thaw cycles on the microscopic damage and macroscopic dynamic properties of rock by nuclear magnetic resonance (NMR). Chen et al. (2015) studied the variation of micro-pores of concrete in a freeze-thaw environment by CT scanning technique. However, the above research results are mostly limited to the mesoscopic freeze-thaw damage identification of a specific area or a particular scanning section of the rock sample and lack of intuitive analysis of the three-dimensional information of the sample. However, the above research results are mostly limited to the freeze-thaw damage identification on some sections of rock, and lack of intuitive analysis of three-dimensional information. The three-dimensional reconstruction technology can more accurately and truly reflect the internal microstructure of rock. Yu et al. (2018) and Ju et al. (2018) considered the real mesostructure of materials, reconstructed the concrete and sand-gravel mixture, and compared the numerical simulation results with the physical experimental results to verify the effectiveness of the method. Wang et al. (2019) reconstructed the mesoscopic geometric coal-rock model and explored the relationship between coal deformation and water migration. Zhao et al. (2020) used nano-CT to reconstruct and characterize nano-pores in coal and simulated the influence of nano-pore structure on coal strength characteristics. Du et al. (2021) carried out CT scanning experiments on raw coal and sandstone, and obtained the damage and energy evolution law according to the three-dimensional reconstruction model of the coal-rock combination. Wang et al. (2021) reconstructed six different coal structure models and carried out a numerical simulation of temperature-pressure coupling using Ansys software. Luo et al. (2022) and Zhang et al. (2022) studied the rare earth ore and shale, obtained the structural characteristics of ore bodies by reconstruction calculation, and studied the relationship between pore characteristics and ore body permeability.

To sum up, the application of three-dimensional reconstruction technology in geotechnical engineering mainly focused on identifying internal information of regular-temperature rock and rock-like materials. However, there are few studies on its combination with rock freeze-thaw damage. The research objects also use sandstone, shale, and other rock samples for testing, and there are few studies on skarn with low porosity and water content. Therefore, this paper takes a metal mine in Xinjiang as the research background, selects the skarn of the surrounding rock of the metal mine as the research object, and studies the damage degradation problem under the freeze-thaw state. Using CT scanning technology and three-dimensional reconstruction technology, the three-dimensional structure digital model of skarn is established, and its internal structure development law is analyzed. The box-counting algorithm is used to calculate the fractal dimension and characteristics of the pore structure of skarn under freeze-thaw conditions. Effective bearing area reduction is used to define the rock damage variable, and the quantitative description of freeze-thaw damage is realized.

2. SAMPLES AND METHODS

2.1 SAMPLE PREPARATION AND EXPERIMENTAL APPARATUS

In this experiment, rock samples were taken from a mine in Xinjiang. The rock samples were cut and smoothed into standard cylindrical rock samples with a diameter of 50 mm and a height of 100 mm. The preparation process was carried out following the international rock mechanics test specifications. Three skarn samples were prepared, numbered xk1, xk2 and xk3 in Fig. 1a.

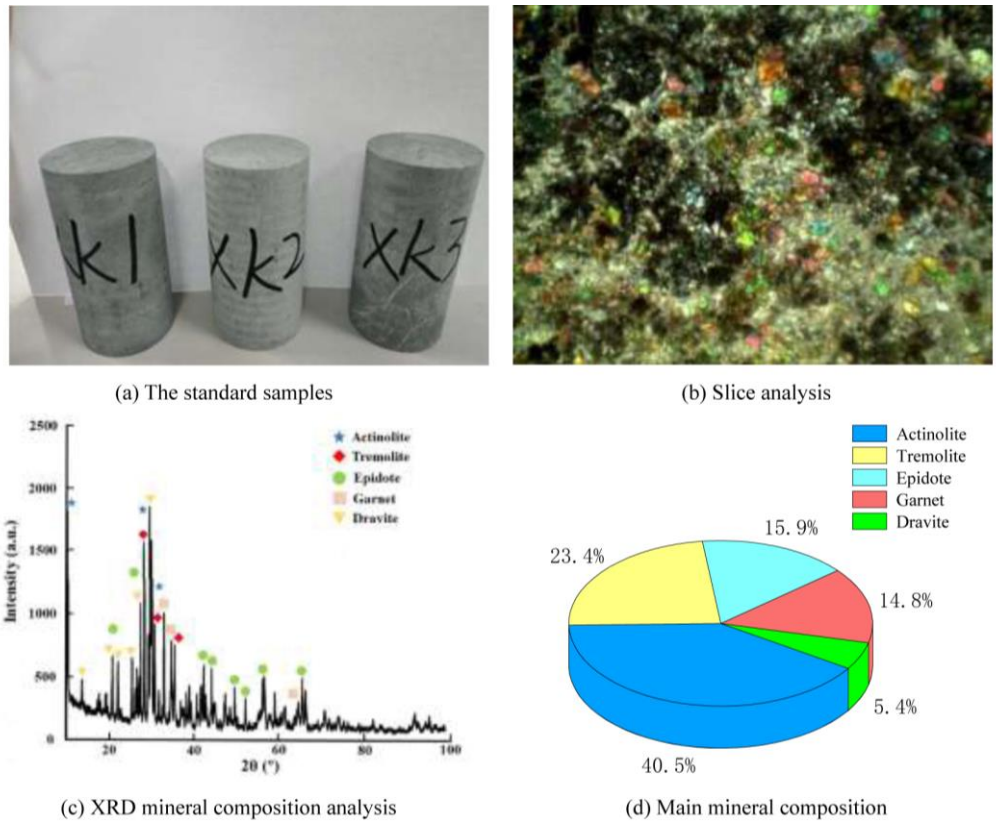

Fig. 1. Skarn mesostructure and mineral composition

The skarn is mainly characterized by porphyritic structure and fibrous structure. The mineral grain size is different. The main minerals are actinolite (40.5%), tremolite (23.4%), epidote (15.9%), garnet (14.8%), dravite (5.4%) and other minerals, as shown in Fig. 1; the uniaxial compressive strength of the rock is 91 MPa, and the tensile strength is 10.8 MPa, which belongs to hard rock.

The freeze-thaw cycle test was carried out in the rapid freeze-thaw machine of the College of Mechanics and Building Engineering of China University of Mining and Technology (Beijing). The freeze-thaw temperature and cycle of the testing machine are controlled by the touch screen controller. The freeze-thaw cycle test process does not need to be carried out manually. After setting the temperature, the test will be carried out completely independently. The time required for one freeze-thaw cycle is 4–6 hours, and the freeze-thaw temperature range is –20 °C–7 °C. According to the local climatic conditions, the temperature in autumn and winter is below zero, the lowest temperature is –40 °C, and the summer varies between 5–15 °C. The freezing temperature of the freeze-thaw machine is –20 °C, the melting temperature is 7 °C, and the freeze-thaw cycle is 4.5 hours.

The ACTIS300-320/22 microfocus X-ray CT scanning equipment was used in the rock CT scanning test instrument. The equipment is from the State Key Laboratory of Coal Resources and Safe Mining of China University of Mining and Technology (Beijing). The scanning spacing is 0.05 mm, the resolution is 1024 × 1024 pixels, and the image bit depth is 16 bit. Skarn specimens before freeze-thaw test and after reaching a specific number of freeze-thaw cycles (25, 50,75 and 100) were subjected to CT scanning test. The leading test equipment is shown in Fig. 2.

Fig. 2. Main equipment used: (a) Freeze-thaw machine,
(b) Micro Focus X-ray CT Scanning Equipment

2.2. OBTAINING 2D CT IMAGES

The original image file obtained by the CT scanning test is converted into a TIF format file, and the CT images of each scanning layer of skarn at 0, 25, 50, 75 and 100 freeze--thaw cycles are obtained. In this paper, firstly, the gray distribution in CT image data is studied, and the gray difference of pixels at different positions in the image is observed. Taking the 990th layer image of xk3 as an example, this layer image's hori-

zontal path gray value is observed. The image gray histogram is shown in Fig. 3. Position A is the crack, and position B is the rock mineral, as shown in Fig. 4a. The gray change of pixels along the horizontal path of the straight line is shown in Fig. 4b. The abscissa represents the distance from left to right of the straight line, and the ordinate represents the gray value of pixels at different distances.

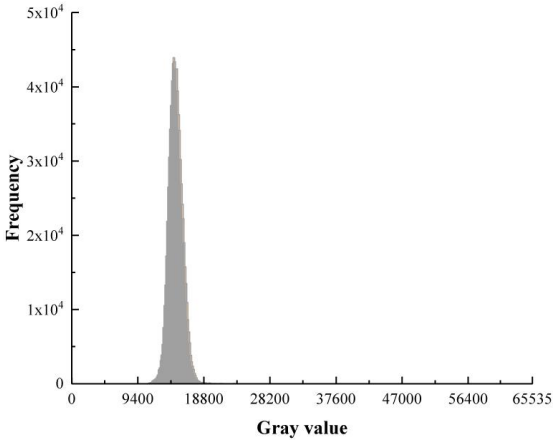

Fig. 3. CT image grayscale histogram

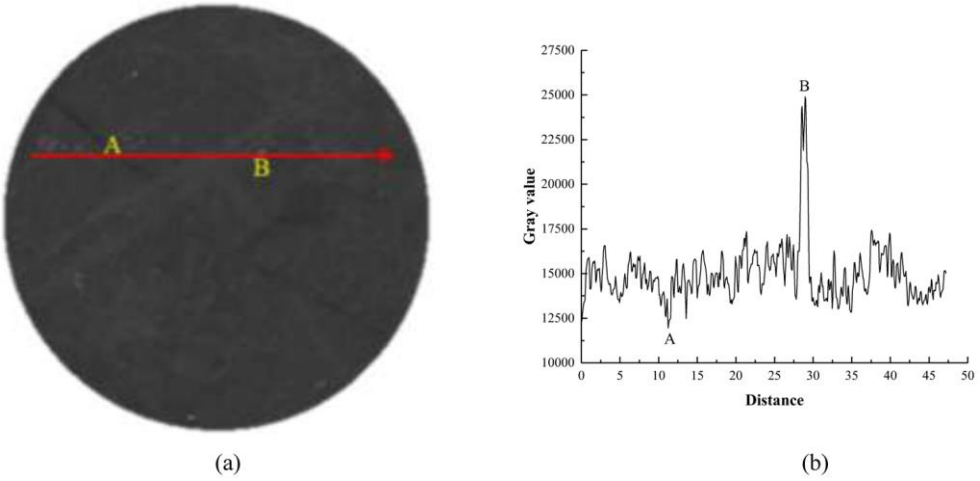

Fig. 4. Image gray value change characteristics along the horizontal path

It can be seen from Fig. 4b that the gray value of the image fluctuates, and there are peaks and troughs in the curve. The differences in grayscale values in CT images re-

flect variations in density, with discrepancies in internal rock density signifying distinct mineral components. Consequently, grayscale images provide a more intuitive means of understanding the evolution characteristics of the rock's mesostructure. Typically, higher grayscale values indicate greater material density, representing mineral components with higher internal rock density. Conversely, lower grayscale values denote lower density, often indicating the presence of microfractures within the rock. When it is located in the low density of holes and cracks (A), the corresponding gray curve trough; when it is located in high density rock minerals (B), the peak of the gray scale curve is corresponding; it is located in the horizontal section with less fluctuation between the peak and the trough, representing the rock particle matrix.

2.3. IMAGE SEGMENTATION AND RECONSTRUCTION

The CT image of frozen-thawed rock obtained by the CT test is two-dimensional. The actual rock is a three-dimensional object. The two-dimensional image can only observe a specific area or multiple scanning sections of the rock sample. It is usually regarded as simplifying the actual three-dimensional model under certain conditions. Although the processing and analysis from the two-dimensional level can reflect its characteristics to a certain extent, there are inevitable limitations. In order to reflect the spatial distribution and morphology of the mesostructure inside the frozen-thawed rock and analyze the three-dimensional damage changes inside the rock, it is necessary to reconstruct the two-dimensional CT image. Avizo software is a visualization software specifically for material science. It uses innovative and efficient algorithms to process and analyze slice data, such as X-ray CT, NMR, MRT equipment, three-dimensional ultrasound equipment, FIB-SEM, and FIM. It performs accurate three-dimensional reconstruction. Therefore, this paper uses Avizo software to establish a three-dimensional structure model of skarn freeze-thaw, accurately distinguish the pore structure, rock matrix, and mineral composition inside the rock sample, and study the damage expansion mechanism of skarn affected by freeze-thaw.

In this study, image processing and analysis were conducted using Avizo software. Initially, the images were subjected to filtering to eliminate noise interference. Subsequently, binary segmentation of the images was performed using the threshold values determined through the maximum between-cluster variance (Otsu) method and fitting method (Ma and Chen 2014). The segmentation thresholds of the three rock samples are 14 225, 11 386, and 12 852, respectively. The segmentation thresholds of the rock matrix and mineral composition are 18 050, 13 786, and 15 670, respectively, and the cracks, matrix, and mineral composition of the skarn sample are segmented accordingly. The segmentation effect is shown in Fig. 5. Then the model is reconstructed in three dimensions to obtain the particle structure model, pore-fracture structure model, and mineral structure model of skarn rock. Finally, to simplify the geometric topological relationship of the digital core rock, the PNM (pore network model) module of Avizo

is used to generate the pore network model. The pore network model is based on the principle of the maximum ball method, and the gray value is used to identify the pores and fissures in the image, and it is simplified to the ball rod model. Spheres represent

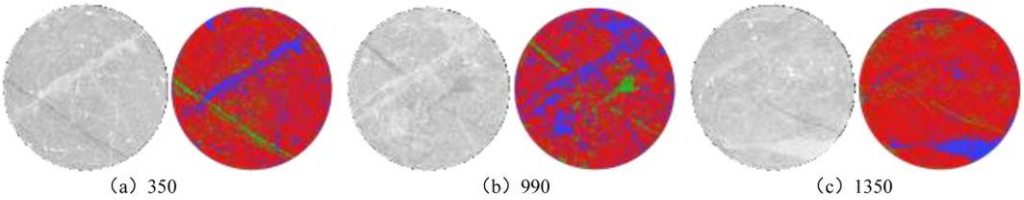

Fig. 5. Threshold segmentation effect comparison chart

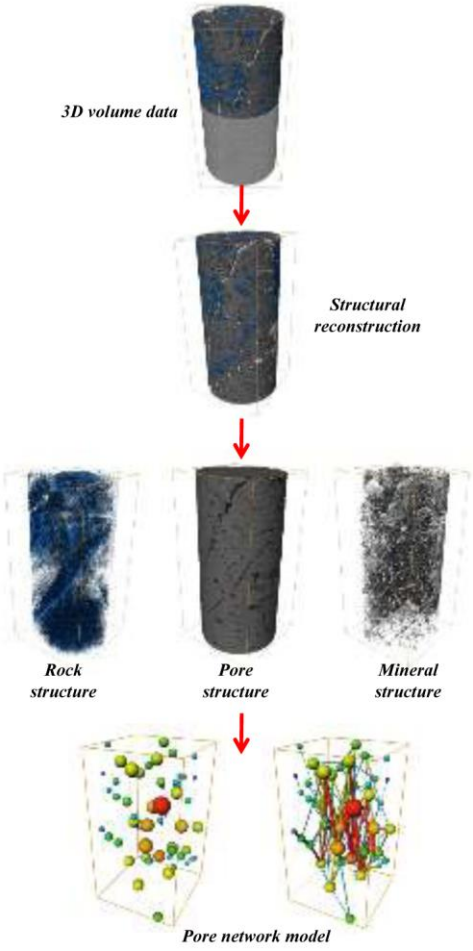

Fig. 6. 3D structural model of skarn

the pores in the digital core, and sticks represent the pore throats in the core. Different sizes of spheres represent different apertures, while different lengths of sticks represent different pore throats, as shown in Fig. 6.

In Figure 5, the green part is a fissure, the blue part is mineral, and the rest is a rock matrix. It can be seen from the comparison in the figure that the mineral and fracture distribution area obtained by threshold segmentation are approximately consistent with the gray-scale image. In the three-dimensional visualization model shown in Fig. 6, blue represents the fracture structure, gray represents the rock particles, and white represents the mineral inclusions. The model's upper half is divided into a three-dimensional reconstruction model, and the lower half is divided into the original rock sample. It is found that the distribution of fractures and minerals in the model is consistent with that of skarn samples.

The three-dimensional reconstruction of the skarn structure model can intuitively show the actual microscopic pore structure development and the spatial distribution of each medium in the rock sample during the freeze-thaw cycle. However, to further study the development law of pores and damage evolution, it is necessary to further quantitatively analyze the rock's internal structure.

3. RESULTS AND DISCUSSION

3.1. STATISTICAL CHARACTERISTICS OF MESOSTRUCTURE

Volume fraction and fractal dimension can usually characterize the content and distribution complexity of various structural components in rock. Quantitative analysis of freeze-thaw damage evolution can be achieved by counting the pixel sets of different gray values in CT images. In the analysis of the three-dimensional reconstruction model of skarn, the porosity, the proportion of rock particles, and the proportion of mineral inclusions of the reconstructed model can be obtained by measuring the three structural volumes extracted. The changes in the structure of the skarn samples under different freeze-thaw cycles are shown in Table 1. The mesostructure change curve of the skarn sample is shown in Fig. 7.

Figure 7a–c shows that the structural change trend of each skarn sample is roughly the same. In general, the porosity increases with the number of freeze-thaw cycles, and the rock particles decrease with the number of freeze-thaw cycles. In contrast, the content of rock mineral composition is unchanged. In order to compare and analyze the mesostructure changes of each rock sample more intuitively, the curves of porosity, rock particles, and mineral composition in Table 1 are plotted, respectively. The curves of each structural component of skarn in the process of the freeze-thaw cycle are obtained, as shown in Fig. 7e, f.

As can be seen from Fig. 7e, f, with the increase in freeze-thaw cycles, the variation trend of each structural component of the three skarn samples is roughly the same. The

porosity of each skarn sample is about 3% in the initial state. At the beginning of the freeze-thaw cycle, the frost heave strain caused by pore water is small due to the influence of rock saturation and pore space. The frost heave deformation cannot occur inside the rock, and the overall performance is cold shrinkage. The development of micropores caused by freeze-thaw action is not apparent, which makes the porosity of skarn samples change little.

When the number of freeze-thaw cycles reaches 25–50, the change of porosity increases compared with that before, indicating that with the increase of the number of freeze-thaw cycles, at this time, due to the phase change of water ice, the frost heaving force is generated and increases continuously. The internal pores of the rock begin to develop, extend and gradually expand under the influence of the frost-heaving effect of the phase change of water ice. The porosity of the specimen gradually increases, the pore development rate gradually increases, and the freeze-thaw damage deterioration continues to increase.

When the number of freeze-thaw cycles reaches 50–100 times, the porosity of each skarn sample increases significantly. Because the freeze-thaw cycle significantly weakens the connection between rock particles. The frost-heaving force generated by the water-ice phase transition causes the pores and cracks caused by the early stage to converge and penetrate gradually. The internal cracks of the rock are interconnected, and the new micro-cracks are further expanded and developed. The porosity of the specimen is further increased.

The variation trend of the proportion of rock particles in each skarn sample decreases inversely with the increase of porosity. The decrease rate is low in the initial stage. With the increase of freeze-thaw cycles, the decrease rate increases gradually. At the same time, the proportion of high density mineral composition is unchanged, this is because the frost heave force generated during the freeze-thaw process is insufficient to precipitate the disintegration of the high-density minerals inside the rock. At this time, the freeze-thaw cycle has little effect on high density mineral composition.

Table 1. Statistical table of structural changes during freeze-thaw cycles

Freeze--thaw cycles	xk1			xk2			xk3		
	Porosity [%]	Proportion of rock particles [%]	Proportion of mineral composition [%]	Porosity [%]	Proportion of rock particles [%]	Proportion of mineral composition [%]	Porosity [%]	Proportion of rock particles [%]	Proportion of mineral composition [%]
0	0.86	49.94	49.2	0.85	52.51	46.64	0.89	44.71	54.4
25	1.29	49.61	49.1	1.12	52.27	46.61	1.27	44.63	54.1
50	1.91	49.09	49	1.74	51.7	46.56	2.05	43.85	54.1
75	2.64	48.56	48.8	2.31	51.15	46.54	2.92	43.08	54
100	3.38	48.02	48.6	2.72	50.76	46.52	3.75	42.45	53.8

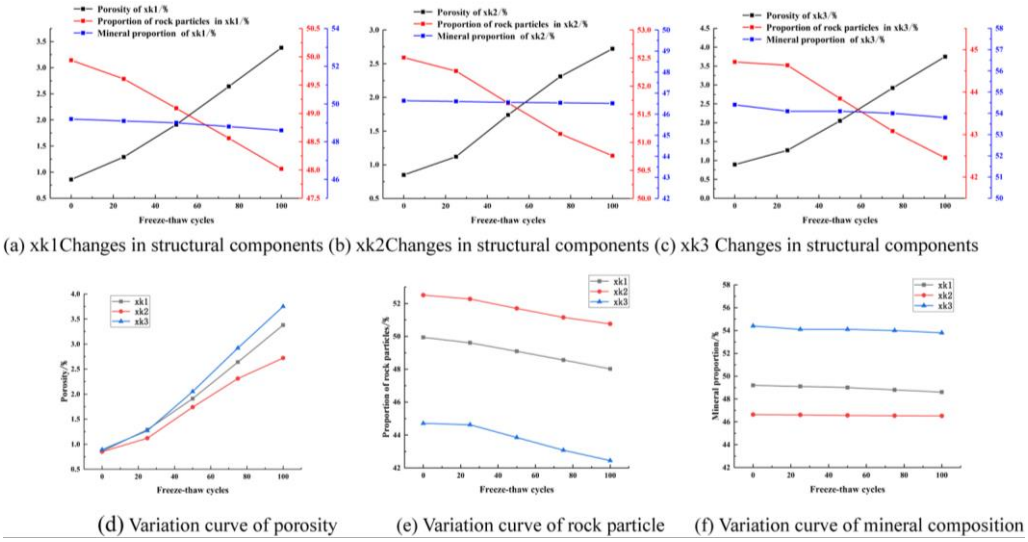

Fig. 7. The curve of meso structure change of skarn sample

3.2. FRACTAL DIMENSION AND PORE SIZE DISTRIBUTION CHARACTERISTICS

Fractal theory has been widely employed to describe and quantify the self-similarity of irregular objects. In their natural state or under laboratory loading conditions, pores and fractures generated by rocks such as coal, shale and sandstone often exhibit strong fractal characteristics (Ai et al. 2014; Ju et al. 2018; Liu et al. 2016). In general, an increase in fractal dimension corresponds to increased irregularity and roughness of the surface, while a decrease in fractal dimension corresponds to enhanced uniformity and smoothness of the surface.

Using the box counting method proposed by the German mathematician Hausdorff in the early twentieth century (Fernández-Martínez and Sánchez-Granero 2012), the fractal dimension of the three-dimensional space of the pore structure in skarn can be obtained. The principle of this method is to cover the target structure with a cube box of side length a and record the required number of boxes $N(a)$. Then use the least square method to fit the relationship between $\lg a$ and $\lg N(a)$ in logarithmic form, where the slope is the fractal dimension D, that is:

$$D = -\lg N(a)/\lg a. \tag{1}$$

The box-counting algorithm determines the rock's two-dimensional and three-dimensional fractal dimensions. Figure 8 shows the two-dimensional fractal dimension of skarn in the vertical direction under the initial state. It can be found that the curve variation trend of the fractal dimension of each skarn is different. The fractal dimension of each scanning slice in the same specimen is also different, indicating that the

complexity of pore structure in different skarns and each skarn is different under the initial state. There are different degrees of initial damage.

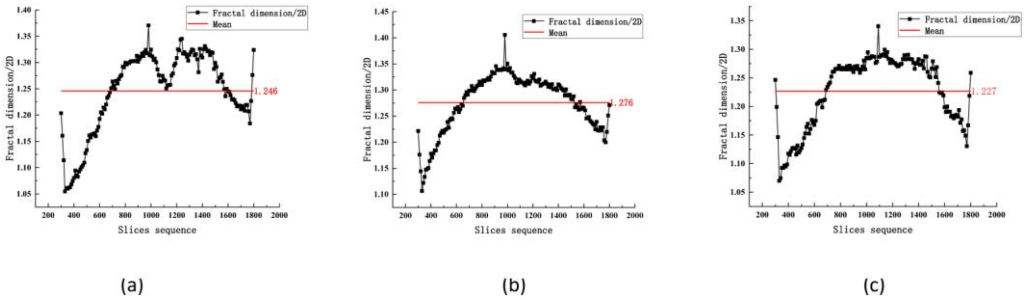

Fig. 8. Fractal dimension/2D variation curve of skarn in the initial state

In the three-dimensional space, the fractal box dimension is between 2 and 3. As the number of fractures increases and the complexity increases, the fractal dimension gradually increases. Table 2 shows the two-dimensional and three-dimensional fractal dimensions of the pore-fissure of each scanning slice of three skarn specimens under freeze-thaw cycles. The two-dimensional fractal dimension mean values of xk1, xk2, and xk3 under different freeze-thaw cycles fluctuate around 1.25, 1.26, 1.38, 1.42 and 1.45, and the three-dimensional fractal dimension values fluctuate at 2.27, 2.34, 2.43, 2.50 and 2.54. The fractal dimension of the rock gradually increases, and the freeze-thaw action leads to different degrees of complex development and expansion of the pore fracture structure in each skarn.

In addition, the two-dimensional and three-dimensional fractal dimension values of skarn in the initial state are xk2 > xk1 > xk3, indicating that the pore structure of xk2 is complex and the pore structure of xk3 is simple in the initial state. With the increase in the number of freeze-thaw cycles, the internal pores of the rock develop, extend and expand to different degrees. After 100 freeze-thaw cycles, the two-dimensional and three-dimensional fractal dimension values of the skarn are no longer the same as the initial state order, indicating the non-uniformity and irregularity of the internal pore structure development of the rock during the freeze-thaw process.

Figure 9a–c shows the variation of fractal dimension and volume fraction of skarn pore structure in the freeze-thaw cycles process. It can be seen that the variation trend of volume fraction and fractal dimension of pores in skarn specimens is roughly the same, and there is a positive correlation between them. Figure 9d shows the curve fitting of the relationship between the three-dimensional fractal dimension of skarn pores and the number of freeze-thaw cycles. Through fitting, it is found that they satisfy the distribution form of the exponential function, and the fitting results are promising, indicating that the exponential function can better describe the nonlinear characteristics of the pore fractal dimension of skarn during the freeze-thaw cycle.

Table 2. Fractal dimension statistics of skarn

Freeze-thaw cycles	xk1			
	Two-dimensional fractal dimension Minimum value	Two-dimensional fractal dimension Maximum value	Two-dimensional fractal dimension Mean value	Three-dimensional fractal dimension
0	1.051	1.371	1.246	2.274
25	1.055	1.372	1.261	2.351
50	1.116	1.454	1.35	2.429
75	1.165	1.488	1.393	2.493
100	1.191	1.516	1.431	2.542
Freeze-thaw cycles	xk2			
	Two-dimensional fractal dimension Minimum value	Two-dimensional fractal dimension Maximum value	Two-dimensional fractal dimension Mean value	Three-dimensional fractal dimension
0	1.092	1.399	1.275	2.313
25	1.107	1.405	1.276	2.354
50	1.177	1.484	1.366	2.443
75	1.239	1.512	1.405	2.494
100	1.267	1.527	1.429	2.524
Freeze-thaw cycles	xk3			
	Two-dimensional fractal dimension Minimum value	Two-dimensional fractal dimension Maximum value	Two-dimensional fractal dimension Mean value	Three-dimensional fractal dimension
0	1.061	1.34	1.227	2.245
25	1.07	1.346	1.239	2.315
50	1.146	1.443	1.342	2.428
75	1.206	1.485	1.397	2.502
100	1.222	1.485	1.4	2.554

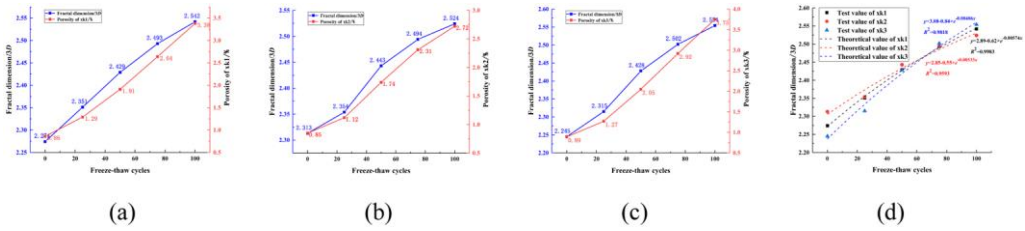

(a) (b) (c) (d)

Fig. 9. Fractal dimension and porosity of rock under freeze-thaw cycles

To reflect the internal pore size distribution characteristics of skarn under freeze-thaw cycles, this study represents the internal fracture structures of rocks in the digital model as easily measurable shapes. In Avizo software, the segmented pore-fracture structures were quantitatively analyzed and processed using “Label Analysis” module. Each independent fracture structure was represented by a sphere with the same vol-

ume, and its equivalent diameter was calculated. The equivalent diameter was determined using Eq. (2):

$$D_{\text{eq}} = \sqrt[3]{6V_p / \pi}\,, \tag{2}$$

where D_{eq} is the equivalent diameter of pore-fissure and V_P is the volume of pore--fissure.

In this paper, under different freeze-thaw cycles, the pore structure models of skarn are counted according to different equivalent diameter ranges. For the convenience of statistics, the pore equivalent diameter of 1.0 mm is used as the boundary value. Below 1.0 mm, every 0.2 mm is divided into five ranges. Above 1.0 mm, 0.5 mm is divided into five ranges. The specific statistical results are shown in Fig. 10.

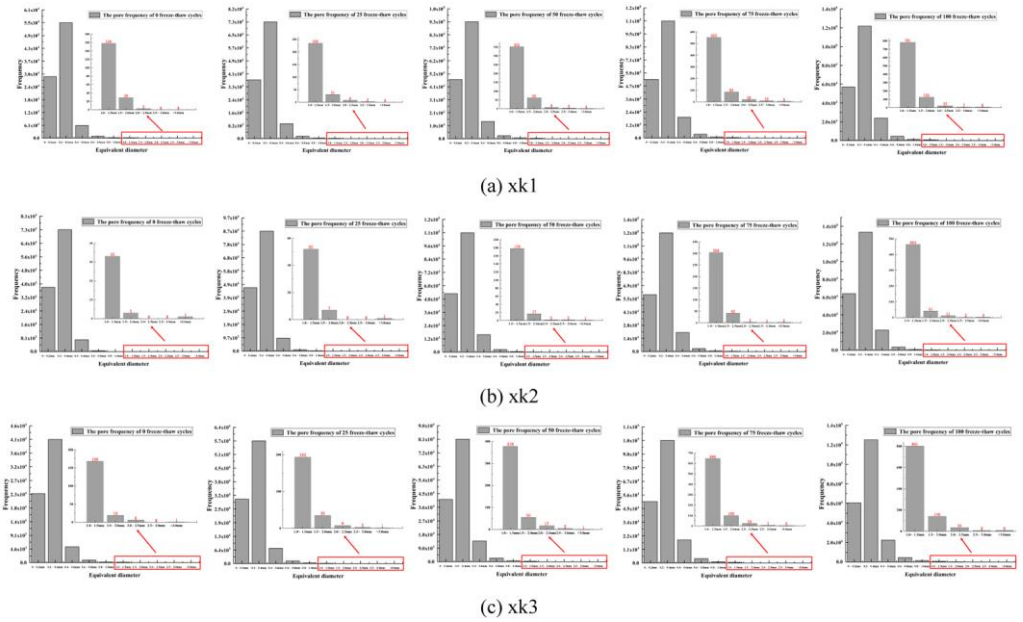

(a) xk1

(b) xk2

(c) xk3

Fig. 10. Statistical results of pore equivalent diameter distribution of skarn under different freeze-thaw cycles

It can be found from the results that the number of pores in $D_{\text{eq}} < 0.4$ mm is the largest, while the number of pores in $D_{\text{eq}} > 1.0$ mm is the smallest. The total number of pores increases first and then decreases with the increase of equivalent diameter. At the same time, with the increase in freeze-thaw cycles, the overall number of pores gradually increases.

The change in the number of pore structures with $D_{\text{eq}} > 1.0$ mm can reflect the development and expansion process of pores inside the skarn under the influence of freeze-

-thaw. In the early stage of freeze-thaw, the number of pores with 1.0 mm < D_{eq} < 2.0 mm increases, and the large pores with D_{eq} > 2.0 mm change relatively minor, and the macroscopic fracture development is not apparent. When the number of freeze-thaw cycles reaches 50 times, the water migration in the water ice phase transition and melting stage during the freezing process makes the pore-fracture inside the rock sample begin to develop and extend. The number of macropores with D_{eq} > 2.0 mm increases, and the number of macro-microcracks increases.

As the number of freeze-thaw cycles further increases, the micro-cracks caused by the early stage gradually expand, and the internal cracks are connected so that the number of pores with D_{eq} > 3.0 mm gradually increases, forming macroscopic penetrating cracks. The analysis results show that the number of pores with different equivalent diameters in the skarn is consistent with the variation of the pore volume fraction of the skarn.

3.3. QUANTITATIVE ANALYSIS OF DAMAGE EVOLUTION

In order to further study the damage evolution of skarn samples during the freeze-thaw process, from the perspective of damage mechanics, the concept of effective bearing area reduction is used to define the damage variables of skarn samples under the freeze-thaw environment as follows:

$$D = 1 - \frac{V_e}{V}. \tag{3}$$

In Equation (3), D is the damage variable, and the range is 0 ~ 1, V_e is the effective bearing volume, mm^3; V is the nominal bearing volume, mm^3.

The nominal bearing volume is divided into three parts: rock particle volume, mineral volume, and pore volume, and the effective bearing area is the two parts of rock particle volume and mineral volume. At the same time, because the rock naturally contains various defects, that is, initial damage, considering the removal of the influence of initial damage, the above formula can be changed into :

$$D = \frac{V_V - V_{V0}}{V_V + V_S + V_T - V_{V0}}. \tag{4}$$

In Equation (4), V_V is pore volume, mm^3; V_S is the volume of rock particles, mm^3; V_T is mineral volume, unit mm^3; V_{V0} is the initial pore volume, mm^3.

According to Eq. (4), the damage variables of each skarn sample during the freeze-thaw cycle are calculated, as shown in Table 3. The relationship curve between the damage variable and freeze-thaw cycles is drawn, as shown in Fig. 11.

From Table 3 and Fig. 11, it can be seen that the trend of the change curve of the damage variable of the above three skarn samples is roughly the same, indicating that the

change rule of the damage variable of skarn under different freeze-thaw cycles is as shown in Fig. 11. However, the damage variable of each skarn sample is different under different freeze-thaw cycles. Because there are different initial damages inside the rock, and the damage area distribution of each skarn sample is not the same. Under the same freeze-thaw cycle conditions, the internal damage evolution of each skarn is inhomogeneous, so the damage variables are different.

Table 3. Statistical table of damage variables of each rock sample under freeze-thaw cycle conditions

Freeze-thaw cycles	Damage variable of xk1	Damage variable of xk2	Damage variable of xk3
0	0	0	0
25	0.00434	0.00272	0.00383
50	0.01059	0.00898	0.01171
75	0.01795	0.01473	0.02048
100	0.02542	0.01886	0.02886

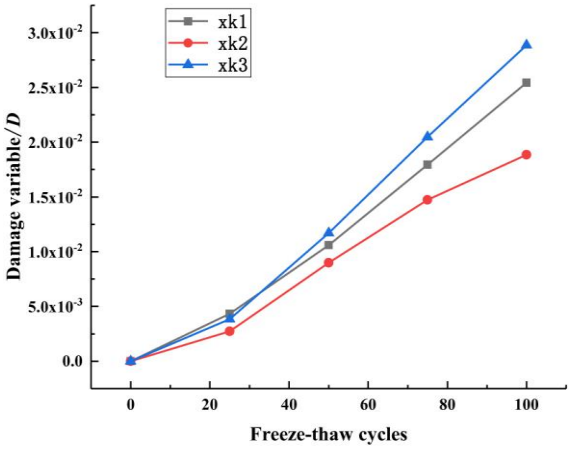

Fig. 11. Variation curve of damage variables of each skarn sample

In previous studies, the evolution model of freeze-thaw damage variables with the number of freeze-thaw cycles has a linear form, exponential form, and logarithmic function form (Liu et al. 2015; Feng et al. 2022; Gao et al. 2020). According to the test data and function characteristics, the exponential function in the form of $D(n) = a \cdot (1 - b^n)$ can better describe the damage evolution law and the nonlinear characteristics of rock in the freeze-thaw process. The relationship between the damage variable of each skarn sample and the number of freeze-thaw cycles and the fitting curve is obtained by fitting, as shown in Fig. 12.

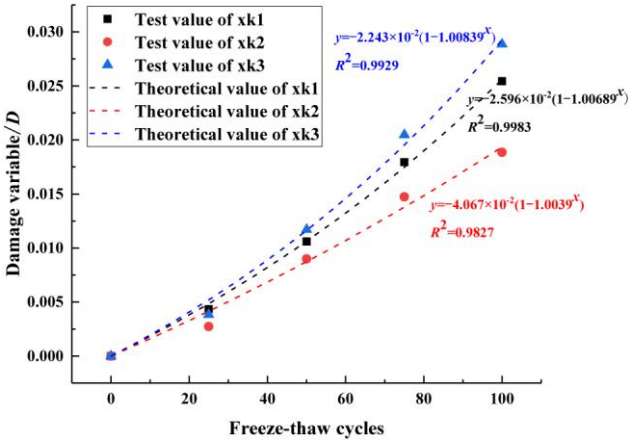

Fig. 12. Fitting curve of skarn damage variable and freeze-thaw times

It can be seen from Fig. 12 that the theoretical curve between the freeze-thaw damage variable and the number of freeze-thaw cycles is in good agreement with the experimental value, indicating that the exponential function can better describe the damage evolution law of skarn after freeze-thaw cycles.

From Figures 11 and 12, the changing trend of the skarn damage variable under freeze--thaw action is nonlinear, and the damage change rate under different freeze-thaw stages is different. In the early stage of freeze-thaw cycles, the rock particles are closely arranged, the porosity of the sample is minor, and the pore development is slow, so the damage variable value and the damage variable evolution rate are small. With the increase of freeze-thaw cycles, due to the repeated frost heaving of water ice phase transition and the uneven expansion of rock particles, the pores gradually expand and develop, the damage area increases, and the damage variable increases. After 50 freeze-thaw cycles, the damage variables of each skarn sample increase rapidly, indicating that with the increase in the number of freeze-thaw cycles, the freeze-thaw damage deterioration of skarn increases continuously. The water-ice phase change in the pores and fissures of the rock sample increases the frost-heaving force. The pores and fissures are further expanded, connected, and merged to form a pore space structure, which eventually leads to a further increase in the area of the skarn damaged area, and the freeze-thaw damage variable value and damage evolution rate increase rapidly. The evolution law of the damage variable obtained in this paper is consistent with the increased law of porosity.

4. CONCLUSION

In this paper, the freeze-thaw cycle CT scanning test was carried out on the skarn of the surrounding rock in the mining area. By dividing the gray values of different struc-

tural components in the freeze-thaw rock, the three-dimensional structure digital model of the skarn was reconstructed. The changes of various structural components in the rock during the freeze-thaw cycle were quantitatively analyzed. The relationship between the fractal dimension and the volume fraction of the pore structure under freeze-thaw conditions was studied. According to the statistical results of the pore size distribution characteristics of the skarn, the changes in the pore structure inside the rock under the influence of freeze-thaw were analyzed, and the freeze-thaw damage evolution law of the skarn was explored in combination with the damage mechanics theory. The main conclusions are as follows :

The three-dimensional reconstruction is carried out using Avizo software, which genuinely reflects the spatial distribution and morphology of the mesostructure inside the freeze-thaw rock. The pore structure will increase at different rates with freeze-thaw cycles. The variation trend of rock particle content decreases with the increase of pore structure. The decreasing amplitude is small in the initial stage and gradually increases with the increase of freeze-thaw. In contrast, the rock's mineral composition is unchanged, and the effect of freeze-thaw on rock minerals is not significant.

Under the freeze-thaw cycle, the fractal dimension of the skarn pore structure is positively correlated with the volume fraction, and the exponential function can better describe the nonlinear characteristics of the pore fractal dimension during the freeze-thaw cycles. According to the statistical results of the pore size distribution of skarn, it is found that the number of pores with different pore size distributions increases with the increase of freeze-thaw cycles, which is consistent with the variation of the pore volume fraction of skarn.

According to the theory of damage mechanics, skarn’s mesoscopic damage evolution law was quantitatively analyzed. The results show that the freeze-thaw damage variable of skarn will increase with the freeze-thaw cycle, and the damage evolution rate will continue to increase, which is consistent with the expansion law of pore structure in rock. At the same time, the exponential function can better reflect the mesoscopic damage evolution law of skarn under freeze-thaw action.

ACKNOWLEDGEMENTS

The authors sincerely thank the following financial support for this work: the National Key Research and Development Program of China (2022YFC2904100) and the Open Fund of State Key Laboratory of Coal Resources and Safe Mining of China University of Mining & Technology (Beijing) (NO. SKLCRSM20KFA11).

STATEMENTS AND DECLARATIONS

DECLARATIONS

The authors declare no conflict of interest.

REFERENCE

[1] TAN X., CHEN W., TIAN H. et al., 2011a, *Water flow and heat transport including ice/water phase change in porous media: numerical simulation and application*, Cold Reg. Sci. Technol., 68 (1), 74–84, https://doi.org/10.1016/j.coldregions.2011.04.004

[2] TAN X., CHEN W., WU G. et al., 2011b, *Laboratory investigations on the mechanical properties degradation of granite under freeze-thaw cycles*, Cold Reg. Sci. Technol., 68 (3), 130–138, https://doi.org/10.1016/j.coldregions.2011.05.007

[3] WANG L.P., LI N., QI J.L. et al., 2019, *A study on the physical index change and triaxial compression test of intact hard rock subjected to freeze-thaw cycles*, Cold Regions Science and Technology, 160, 39–47, https://doi.org/10.1016/j.coldregions.2019.01.001

[4] NICHOLSON D.T., NICHOLSON F.H., 2000, *Physical deterioration of sedimentary rocks subjected to experimental freeze-thaw weathering*, Earth Surf. Proc. Land., 25 (12), 1295–1307, https://doi.org/10.1002/1096-9837(200011)25:12<1295::AID-ESP138>3.0.CO;2-E

[5] BAYRAM F., 2012, *Predicting mechanical strength loss of natural stones after freeze-thaw in cold regions*, Cold Reg. Sci. Technol., 83–84, 98–102, https://doi.org/10.1016/j.coldregions.2012.07.003

[6] CARDENES V., MATEOS F.J., FERNANDEZ-LORENZO S., 2014, *Analysis of the correlations between freeze-thaw and salt crystallization tests*, Environ. Earth Sci., 71 (3), 1123–1134. https://doi.org/10.1007/s12665-013-2516-7

[7] ESLAMIA J., WALBERTA Ch., BEAUCOUR A.-L. et al., 2018, *Influence of physical and mechanical properties on the durability of limestone subjected to freeze-thaw cycles*, Construction and Building Materials, 162,420–429, https://doi.org/10.1016/j.conbuildmat.2017.12.031

[8] ZHANG J., DENG H., TAHERI A. et al., 2018, *Degradation of physical and mechanical properties of sandstone subjected to freeze-thaw cycles and chemical erosion*, Cold Reg. Sci. Technol., 155, 37–46, https://doi.org/10.1016/j.coldregions.2018.07.007

[9] QIAO C., WANG Y., TONG Y.J. et al., 2021, *Deterioration characteristics of pre-flawed granites subjected to freeze-thaw cycles and compression*, Geotech. Geol. Eng., 39, 5907–5916. https://doi.org/10.1007/s10706-021-01904-x

[10] YAN X., LIU H., XING C. et al., 2015, *Constitutive model research on freezing-thawing damage of rock based on deformation and propagation of microcracks*, Rock Soil Mech., 36 (12), 3489–3499.

[11] HUANG S., LIU Q., LIU Y. et al., 2018, *Freezing strain model for estimating the unfrozen water content of saturated rock under low temperature*. Int. J. Geomech., 18, 04017137, https://doi.org/10.1061/(ASCE)GM.1943-5622.0001057

[12] LV Z.T., LUO S.C.,·XIA C.C. et al., 2022, *A thermal–mechanical coupling elastoplastic model of freeze-thaw deformation for porous rocks*, Rock Mechanics and Rock Engineering, 55 (6), 3195–3212, https://doi.org/10.1007/s00603-022-02794-y

[13] HUANG S.B., CAI Y.T., LIU Y.Z. et al., 2021a, *Experimental and theoretical study on frost deformation and damage of red sandstones with different water contents*, Rock Mechanics and Rock Engineering, 54, 4163, https://doi.org/10.1007/s00603-021-02509-9

[14] HUANG S.B., XIN Z.K., YE Y.H. et al., 2021b, *Study on the freeze-thaw deformation behavior of the brittle porous materials in the elastoplastic regime based on Mohr–Coulomb yield criterion*, Construction and Building Materials, 268, 121799, https://doi.org/10.1016/j.conbuildmat.2020.121799

[15] GAO F., CAO S., ZHOU K. et al., 2020, *Damage characteristics and energy-dissipation mechanism of frozen-thawed sandstone subjected to loading*, Cold Reg. Sci. Technol., 169, 102920. https://doi.org/10.1016/j.coldregions.2019.102920

[16] WANG Y., GAO S., LI C. et al., 2021, *Energy dissipation and damage evolution for dynamic fracture of marble subjected to freeze-thaw and multiple level compressive fatigue loading*, Int. J. Fatig. 142, 105927, https://doi.org/10.1016/j.ijfatigue.2020.105927

[17] FENER M., INCE I., 2015, *Effects of the freeze-thaw (F–T) cycle on the andesitic rocks (Sille-Konya/Turkey) used in construction building*, J. Afr. Earth Sci., 109, 96–106, https://doi.org/10.1016/j.jafrearsci.2015.05.006

[18] PARK J., HYUN C.U., PARK H.D., 2015, *Changes in microstructure and physical properties of rocks caused by artificial freeze-thaw action*. Bull. Eng. Geol. Env., 74 (2), 555–565, https://doi.org/10.1007/s10064-014-0630-8

[19] ZHOU K.P., ZHOU B., LI J.L. et al., 2015, *Microscopic damage and dynamic mechanical properties of rock under freeze-thaw environment*, Transactions of Nonferrous Metals Society of China, 25 (4), 1254–1261, https://doi.org/10.1016/S1003-6326(15)63723-2

[20] CHEN J.X., DENG X.H., LUO Y.B. et al., 2015, *Investigation of microstructural damage in shotcrete under a freeze-thaw environment*, Construction and Building Materials, 83, 275–282, https://doi.org/10.1016/j.conbuildmat.2015.02.042

[21] YU Q.L., LIU H.Y., YANG T.H. et al., 2018, *3D numerical study on fracture process of concrete with different ITZ properties using X-ray computerized tomography*, International Journal of Solids and Structures, 147, 204–222, https://doi.org/10.1016/j.ijsolstr.2018.05.026

[22] JU Y., SUN H., XING M. et al., 2018, *Numerical analysis of the failure process of soil–rock mixtures through computed tomography and PFC3D models*, International Journal of Coal Science and Technology, 5 (2), 126–141, https://doi.org/10.1007/s40789-018-0194-5

[23] WANG G., JIANG C.H., SHEN J.N. et al., 2019. *Deformation and water transport behaviors study of heterogeneous coal using CT-based 3D simulation*, International Journal of Coal Geology, 211, 103204, https://doi.org/10.1016/j.coal.2019.05.011

[24] DU F., WANG K., DONG X.L. et al., 2021, *Numerical simulation of damage and failure of coal-rock combination based on CT three-dimensional reconstruction*, Journal of China Coal Society, 46 (S1), 253–262.

[25] ZHAO Y.X., SUN Y.F., YUAN L. et al., 2020, *Impact of nano-pore structure on coal strength: A study based on synchrotron radiation nano-CT*. Results in Physics, 17, 103029, https://doi.org/10.1016/j.rinp.2020.103029

[26] WANG G., QIN X.J., ZHOU J.P. et al., 2021, *Simulation of coal microstructure characteristics under temperature-pressure coupling based on micro-computer tomography*, Journal of Natural Gas Science and Engineering, 91,103906, https://doi.org/10.1016/j.jngse.2021.103906

[27] LUO X.P., ZHANG Y.B., ZHOU H.P. et al., 2022, *Pore structure characterization and seepage analysis of ionic rare earth orebodies based on computed tomography images*, International Journal of Mining Science and Technology, 32 (2), 411–421, https://doi.org/10.1016/j.ijmst.2022.02.006

[28] ZHANG J.C., SANG S., MA T.R. et al., 2022, *Shale microstructure extraction based on micro-CT and permeability inversion*, Geotech. Geol. Eng., 40, 3245–3254, https://doi.org/10.1007/s10706-022-02090-0

[29] MA T.S., CHEN P., 2014, *Study of Meso-Damage Characteristics of Shale Hydration Based On Ct Scanning Technology*, Petroleum Exploration and Development, 41 (2), 249–256, https://doi.org/10.1016/S1876-3804(14)60029-X

[30] AI T., ZHANG R., ZHOU H.W. et al., 2014, *Box-Counting Methods to Directly Estimate the Fractal Dimension of a Rock Surface*, Applied Surface Science: A Journal Devoted to the Properties of Interfaces in Relation to the Synthesis and Behaviour of Materials, 314 (Sep. 30), 610–621, https://doi.org/10.1016/j.apsusc.2014.06.152

[31] JU Y., XI C., ZHANG Y. et al., 2018, *Laboratory in Situ CT Observation of the Evolution of 3D Fracture Networks in Coal Subjected to Confining Pressures and Axial Compressive Loads: A Novel Approach*, Rock Mech. Rock Eng., 51 (11), 3361–3375, https://doi.org/10.1007/s00603-018-1459-4

[32] LIU P., JU Y., RANJITH P.G. et al., 2016, *Experimental Investigation of the Effects of Heterogeneity and Geostress Difference On the 3D Growth and Distribution of Hydrofracturing Cracks in Unconventional Reservoir Rocks*, J. Nat. Gas Sci. Eng., 35, 541–554, https://doi.org/10.1016/j.jngse.2016.08.071

[33] FERNÁNDEZ-MARTÍNEZ M., SÁNCHEZ-GRANERO M.A., 2012, *Fractal dimension for fractal structures: A Hausdorff approach*, Topology and its Applications, 159 (7), 1825–1837, https://doi.org/10.1016/j.topol.2011.04.023

[34] LIU Q.S., HUANG S.B., KANG Y.S. et al., 2015, *Fatigue damage model and evaluation index for rock mass under freezing-thawing cycles*, Chinese Journal of Rock Mechanics and Engineering, 34 (6), 1116–1127

[35] FENG Q., JIN J.C., ZHANG S. et al., 2022, *Study on a damage model and uniaxial compression simulation method of frozen–thawed rock*, Rock Mechanics and Rock Engineering, 55, 187–211, https://doi.org/10.1007/s00603-021-02645-2